0888-8809/07/$15.00/0
Printed in U.S.A.

Molecular Endocrinology 21(2):512–523

doi: 10.1210/me.2006-0202

Mapping the Binding Site of Arginine Vasopressin to V_{1a} and V_{1b} Vasopressin Receptors

Jordi Rodrigo,* Ana Pena,* Brigitte Murat, Miguel Trueba, Thierry Durroux, Gilles Guillon, and Didier Rognan

Bioinformatics of the Drug (J.R., D.R.), Centre Nationale de la Recherche Scientifique-Université Louis Pasteur (CNRS-ULP), Unité Mixte de Recherche (UMR) 7175-LC1, F-67401 Illkirch, France; and Institut de Génomique Fonctionnelle (A.P., B.M., M.T., T.D., G.G.), CNRS UMR 5203, Institut National de la Santé et de la Recherche Médicale Unité 661, Universités Montpellier I et II, F-34094 Montpellier Cédex 5, France

Starting from the 2.8-Å resolution x-ray structure of bovine rhodopsin, three-dimensional molecular models of the complexes between arginine vasopressin and two receptor subtypes (V_{1a}, V_{1b}) have been built. Amino acid sequence alignment and docking studies suggest that four key residues (1.35, 2.65, 4.61, and 5.35) fine tune the binding of vasopressin and related peptide agonists to both receptor subtypes. To validate these predictions, a series of single or double mutants were engineered at V_{1a} and V_{1b} receptor subtypes and tested for their binding and functional properties. Two negatively charged amino acids at positions 1.35 and 2.65 are key anchoring residues to the Arg8 residue of arginine vasopressin. Moreover, two amino acids ($V^{4.61}$ and $P^{5.35}$) delineating a hydrophobic subsite at the human V_{1b} receptor are responsible for the recognition of V_{1b} selective peptide agonists. Last, one of the latter positions (5.35) is hypothesized to explain the pharmacological species differences between rat and human vasopressin receptors for a V_{1b} peptide agonist. Altogether these refined three-dimensional models of V_{1a} and V_{1b} human receptors should enable the identification of further new selective V_{1a} and V_{1b} agonists as pharmacological but also therapeutic tools. (*Molecular Endocrinology* 21: 512–523, 2007)

ARGININE VASOPRESSIN (AVP) IS a neurohypophysial nonapeptide hormone that exerts major physiological roles upon binding to three receptor subtypes regulating blood pressure (V_{1a} subtype), ACTH release, stress and anxiety (V_{1b} subtype also named V_3), and water reabsorption in the kidney (V_2 subtype) (1, 2). Both receptor subtypes have been cloned in various species and belong to the wide family of G protein-coupled receptors (GPCRs) characterized by a typical heptahelical transmembrane (TM) domain (3). AVP receptors are prototypes of peptidergic GPCRs (4) able to accommodate significantly different binding modes peptide or nonpeptide ligands (agonists and/or antagonists) and thus are particularly interesting for determining fine molecular features responsible for ligand binding (5). The combination of molecular modeling, covalent labeling, and site-directed mutagenesis (5–14) has shed light on hypothetical binding modes of AVP or close analogs [oxytocin (OT), vasotocin] to their specific receptors, although a clear consensus on the exact binding mode is still missing for two main reasons. First, most recognition models further investigated by site-directed mutagenesis studies have been proposed from either an ancient x-ray structure of bacteriorhodopsin (6, 9), which is not a GPCR, or a low-resolution map of bovine rhodopsin (7, 8, 10–12, 14). Second, three-dimensional models based on the more recent high-resolution x-ray structure of bovine rhodopsin are still lacking experimental validation (15, 16). Although previous models may probably not be used for accurate structure-based design, they have proven their utility to partially map the binding site of AVP. AVP is a nonapeptide (CYFQNCPRG-NH_2) exhibiting a 20-membered tocin ring resulting from a disulfide bridge between both cysteine residues. The conclusion of most studies is that the hydrophobic part of the molecule is accommodated by an hydrophobic pocket ($Met^{3.36}$, $Trp^{6.48}$, $Phe^{6.51}$) lying deep in the 7-TM cavity between TMs III, V, VI, and VII, whereas conserved glutamine residues ($Gln^{2.61}$, $Gln^{3.32}$, $Gln^{4.60}$, $Gln^{6.55}$) located at the rim of the cavity H bonds to the polar part of the peptide hormone (main chain atoms as well as Gln4 and Asn5 side chains) (8, 9). Last, the C-terminal amidated tripeptide probably projects toward a region between TMI and the second extracellular loop (8, 9). Therefore, there is a consensus about the critical receptor residues important for AVP recognition and binding but not on the precise molecular interactions developed by each of the

First Published Online November 2, 2006

* J.R. and A.P. contributed equally to this work.

Abbreviations: AVP, Arginine vasopressin; CHO, Chinese hamster ovary; 3-D, three dimensional; d[Cha^4]AVP, [desamino-cys1]-cyclohexylalanine-4 arginine vasopressin; dDAVP, [desamino-cys1]-DArg-8 vasopressin; GA, genetic algorithm; GPCR, G protein-coupled receptor; HBS, Hanks' buffered saline; IP, inositol phosphate; MD, molecular dynamics; OT, oxytocin; rmsd, root mean square deviation; TM, transmembrane.

***Molecular Endocrinology* is published monthly by The Endocrine Society (http://www.endo-society.org), the foremost professional society serving the endocrine community.**

AVP amino acids. Starting from recent three-dimensional (3-D) models of both V_{1a} and V_{1b} receptors that are able to accurately predict the binding mode of nonpeptide antagonists (17–19), we herewith present a high-resolution model of AVP in complex with each of its two receptor subtypes. Proposed 3-D models, compatible with most known experimental data, have been successfully challenged by site-directed mutagenesis focusing on yet undisclosed peptide-receptor interactions. Binding and functional properties of six mutants of the V_{1a} or the V_{1b} human receptor were investigated using either AVP or the recently described d[Cha^4]AVP analog exhibiting a nice V_{1b} selectivity profile for human vasopressin receptor subtypes (20).

RESULTS

3-D Molecular Modeling

Aligning the amino acid sequences of vasopressin/OT receptors with that of bovine rhodopsin is rather straightforward because rhodopsin-like fingerprints (21, 22) are common to all entries (Fig. 1). The modeled structure of V_{1a} and V_{1b} receptor subtypes, although simulated in an explicitly hydrated phospholipid membrane, remains quite close to the x-ray structure of bovine rhodopsin [root mean square deviation (rmsd) on backbone TM residues between 1.2 and 1.3 Å]. AVP adopts a rather similar binding mode to both V_{1a} and V_{1b} receptor models (Fig. 2 and Table 1), which recalls earlier binding modes described by Mouillac *et al*. (8) and Thibonnier *et al*. (9). With respect to the starting conformation taken from the structure of neurophysin-bound OT (23), a β-turn is still observed in AVP but shifted from positions 2–5 to positions 3–6. Interestingly, the receptor-bound conformation of AVP to V_{1a} and V_{1b} receptor subtypes is similar to that recently proposed for density functional theory (DFT)-optimized Zn^{2+}-bound OT (24) (rmsd of 0.8 Å on backbone atoms of the tocin ring). Carbonyl moieties at positions 2, 3, 6, and 8 converge toward a common region that could accommodate a dicationic ion, as proposed for OT (24).

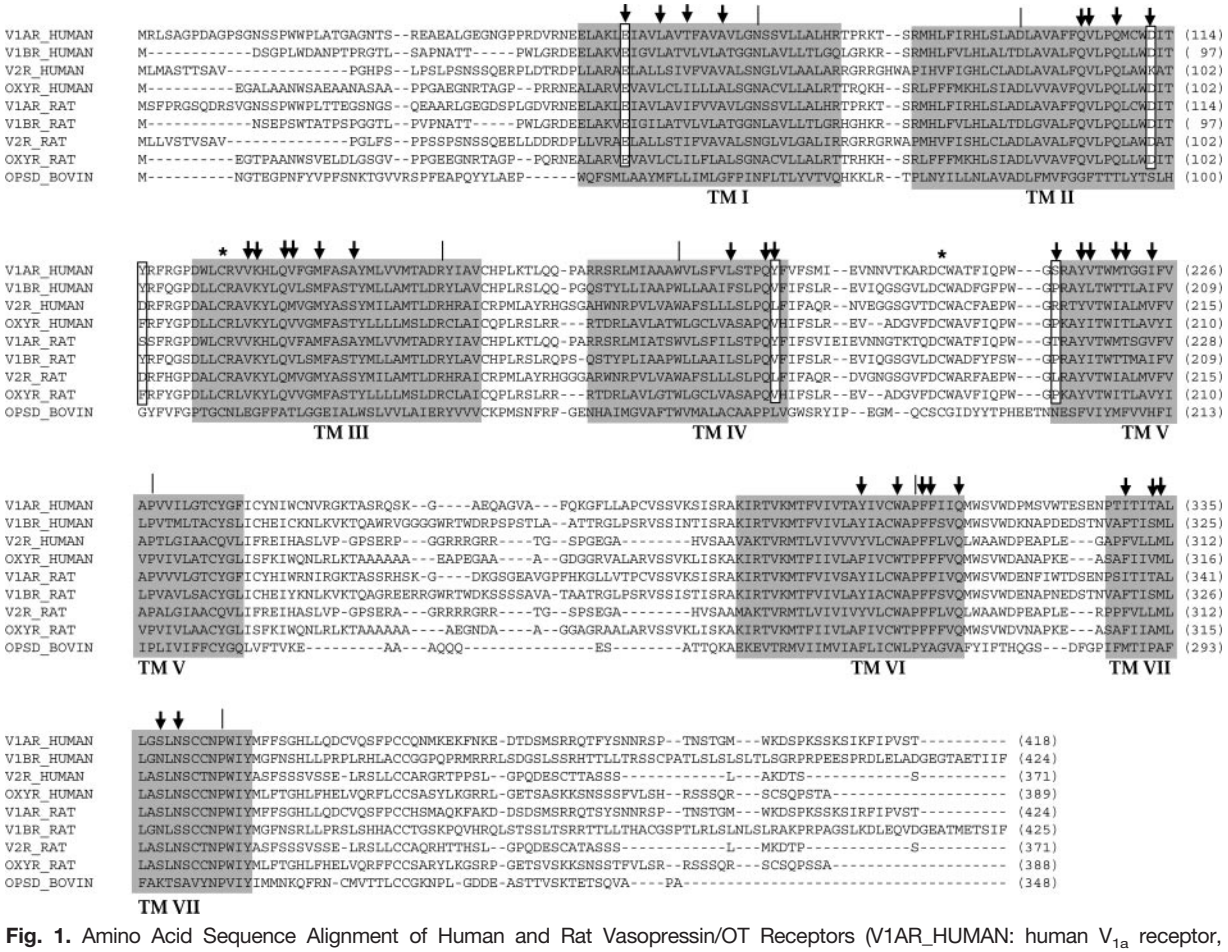

Fig. 1. Amino Acid Sequence Alignment of Human and Rat Vasopressin/OT Receptors (V1AR_HUMAN: human V_{1a} receptor, V1BR_HUMAN: human V_{1b} receptor, V2R_HUMAN: human V_2 receptor, OXYR_HUMAN: human OT receptor, V1AR_RAT: rat V_{1a} receptor, V1BR_RAT: rat V_{1b} receptor, V2R_RAT: rat V_2 receptor, OXYR_RAT: rat OT receptor) to Bovine Rhodopsin (OPSD_BOVIN)

Transmembrane helices (TMI–TMVII) are delimited by *gray boxes*. Amino acids residues mutated in this work are enclosed by *white boxes*. *Down arrows* indicate residues pointing inwards the TM binding cavity (37). Position 50 in Ballesteros numbering (27) of each TM is marked by a *vertical bar*.

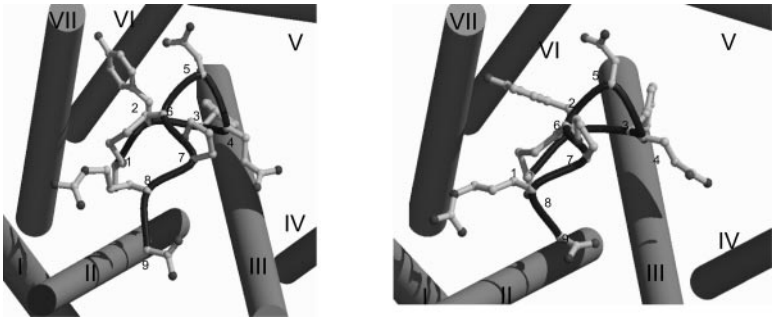

Fig. 2. Proposed Binding Mode of AVP to Human V_{1a} (*Left Panel*) and V_{1b} (*Right Panel*) Receptors

The seven TM helices of each receptor are displayed by *cylinders* and labeled from I–VII. The AVP main chain and side chain atoms are displayed by a *dark tube* and *ball-and-sticks*, respectively. AVP residues are labeled from 1–9. This figure (as well as Figs. 3 and 7) has been prepared with MOLSCRIPT (35) and rendered with Raster3D (36).

A full description of intermolecular interactions between AVP and both receptor subtypes is listed in Table 1. A very tiny network of hydrogen bonds (16–20 H bonds) is used to anchor AVP to its receptor subtypes. Most residues proposed to participate in AVP binding have been shown to be of crucial importance for agonist peptide binding (8–11). Key features of the proposed models involve hydrophobic interactions of Tyr2 side chain with a first apolar pocket between TMVI and TMVII, and of Phe3 aromatic ring with an apolar pocket delineated between TMIII and TMVI. Important hydrogen bonds are established between Gln4 side chain and $Q^{4.60}$, Asn5 side chain, and $Q^{6.55}$ for anchoring the tocin ring to the transmembrane cavity (Table 1). By opposition to previously described models (8, 9), a well-defined negatively charged subsite ($E^{1.35}$, $D^{2.65}$) perfectly accommodates the positively charged Arg8 side chain (Fig. 3, A and B). It should be noted that neither $Y115^{2.68}$ (V_{1a}) nor $Y98^{2.68}$(V_{1b}) was found to interact with Arg8 side chain, as proposed in earlier 3-D models (8, 10).

$E^{1.35}$ and $D^{2.65}$ Are Key-Anchoring Residues in V_{1a} and V_{1b} Receptor Subtypes

The herein proposed molecular models were first challenged by probing the yet undisclosed molecular partner of residue Arg8 of AVP. Three V_{1b} receptor mutants ($E37A^{1.35}$, $D95A^{2.65}$, $Y98A^{2.68}$) have been engineered and tested for their binding properties for [^{3}H]AVP (Fig. 4). As illustrated in Table 2, the three V_{1b} mutants expressed on Chinese hamster ovary (CHO) membranes exhibited maximal binding capacities (B_{max}) around 0.5 pmol [^{3}H]AVP specifically bound per mg protein. These B_{max} values were lower than those found for wild-type V_{1b} receptor. As predicted, mutation of $E37A^{1.35}$ dramatically decreased the affinity of the V_{1b} receptor for [^{3}H]AVP by nearly a factor of 50, thus confirming its utmost importance for AVP recognition. Mutation of the secondary Arg8-contacting residue ($D95^{2.65}$) was less spectacular but nevertheless still significant (4-fold decreased affinity, Table 2). Finally, the $Y98A^{2.68}$ mutation, occurring at TMII-e1 (first extracellular loop) junction, did not changed the affinity of the mutant for [^{3}H]AVP with respect to the wild-type receptor, confirming thus that the latter residue is not involved for AVP recognition to the V_{1b} receptor. Competition experiments using [^{3}H]AVP as radiolabeled ligand and a set of selective V_{1b} unlabeled analogs showed that mutating $E37^{1.35}$ by alanine profoundly affected the pharmacological profile of this V_{1b} mutant. Its affinity for the two peptidic V_{1b} agonists tested (d[Cha^4]AVP, dDAVP) was decreased by at least 135-fold. Moreover its affinity for the nonpeptidic V_{1b} antagonist SSR149415 also dramatically decreased (K_i $>$10,000 nM). $D95A^{2.65}$ mutation had a weaker effect on the pharmacological profile of this mutant. Whereas the affinity of d[Cha^4]AVP was decreased by a factor of 9, that of dDAVP was increased by a factor of 2 (Table 3). As previously noted for AVP, mutation of $Y^{2.68}$ did not strongly affect the pharmacological profile of this mutant for either peptide agonists or nonpeptide antagonists tested herein. Only slight increases of K_i for d[Cha^4]AVP, dDAVP, and SSR149415 were observed as compared with V_{1b} wild-type receptor.

The functional properties of $E37^{1.35}$A and $D95^{2.65}$A V_{1b} mutants transiently expressed in CHO cells were further evaluated by testing their abilities to stimulate inositol phosphate (IP) accumulation. Functional properties of both V_{1b} mutant receptors mirrored their binding properties with a parallel decrease of their affinity constant (K_{act}) for AVP (373 and 41 nM for $E37^{1.35}$A and $D95^{2.65}$A mutants, respectively) compared with V_{1b} wild-type receptor (K_{act}= 0.88 nM for AVP, Table 4).

Residues 4.61 and 5.35 Control the Fine Specificity of d[Cha^4]AVP to V_{1a} and V_{1b} Receptors

Our 3-D models were then used to find a plausible explanation to the previously described nice selectivity profile of d[Cha^4]AVP, a desamino-cys-1 analog of AVP bearing a cyclohexylalanine side chain at position 4 (20). In contrast to AVP, which does not distinguish V_{1a} from V_{1b} subtype with regard to binding affinity,

Table 1. List of Human V_{1a} and V_{1b} Receptor Residues in Close Contacts with AVP

AVP	V_{1a}-R	V_{1b}-R	Numbering[a]
Cys1.N[b]		*Gln87.OE1*	2.57
	Ser338.OG	*Asn328.OD1*	7.43
	Asn340.OD1	*Asn330.OD1*	7.45
Cyx1.sc[c]	Ala334.sc	Met324.sc	7.39
	Leu335.sc	Leu325.sc	7.40
Cyx1.O	*Asn340.ND2*		7.45
Tyr2.O	*Gln131.NE2*	*Gln114.NE2*	3.32
Tyr2.sc	Ala334.sc	Met324sc	7.39
	Phe307.sc	Phe297.sc	6.51
	Ile310.sc		6.54
	Trp304.sc	Trp294.sc	6.48
Tyr2.OH	*Thr333.O*	*Ser323.O*	7.38
Phe3.N			3.32
Phe3.sc	Val132.sc	Val115.sc	3.33
	Met135.sc	Met118.sc	3.36
	Phe136.sc	Phe119.sc	3.37
	Met220.sc		5.42
Phe3.sc	Trp304.sc	Trp294.sc	6.48
	Phe307.sc	Phe297.sc	6.51
Phe3.O	*Gln131.NE2*		3.32
Gln4.OE1	*Lys128.NZ*		3.29
	Tyr186.OH		4.61
		Arg175.NH1	e2[d]
Gln4.NE2	*Gln185.OE1*	*Gln168.OE1*	4.60
Asn5.OD1	*Gln311.NE2*	*Gln301.NE2*	6.55
Asn5.ND2	*Gln311.OE1*	*Gln301.OE1*	6.55
Cys6.O	Gln131.NE2	*Gln114.NE2*	3.32
		Lys111.NZ	3.29
Cys6.sc	Ala334.sc	Met324.sc	7.39
	Leu335.sc		7.40
Pro7.sc	Trp204.sc	Trp187.sc	e2
Pro7.O	*Lys128.NZ*	*Lys111.NZ*	3.29
	Cys203.N	*Cys186.N*	e2
Arg8.N	*Asp202.OD2*	*Asp185.OD2*	e2
Arg8.NE	*Glu54.OE1*	*Glu37.OE1*	1.35
Arg8.NH1	*Asp112.OD2*	*Asp95.OD2*	2.65
Arg8.NH1		*Gln91.OE1*	2.61
Arg8.NH2	*Glu54.OE1*	*Glu37.OE1*	1.35
	Asp112.OD2	*Asp95.OD2*	2.65
Gly9.0	*Lys128.NZ*	*Lys111.NZ*	3.29

[a] Ballesteros numbering (27).
[b] H bonds with interacting atoms are indicated in *italic*.
[c] Side chain (sc) hydrophobic/aromatic contacts.
[d] Second extracellular loop.

d[Cha[4]]AVP exhibits a much stronger affinity for the human V_{1b} receptor than for the human V_{1a} subtype (Table 3). A previous report demonstrated that a hydrophobic side chain at position 4 is clearly responsible for the favored binding to the human V_{1b} subtype (20). Modeling the complex between the latter AVP analog and V_{1a}/V_{1b} receptor subtypes did not reveal major changes in the binding mode with respect to the previously described recognition model of endogenous AVP. A close-up view of amino acids contacting the Cha4 side chain provides a reasonable explanation for the selectivity profile of d[Cha[4]]AVP. When bound to the human V_{1b} receptor, the cyclohexylalanine side chain is nicely embedded in a hydrophobic subsite delimited by $K^{3.29}$, $V^{3.33}$, A188 (e2 loop), $Q^{4.60}$, $V^{4.61}$, $P^{5.35}$, and $Y^{5.38}$ (see Fig. 8). Among these seven residues, five are fully conserved across human V_{1a}/V_{1b} subtypes (Fig. 1) and therefore cannot be invoked to explain the peculiar binding properties of d[Cha[4]]AVP to the V_{1b} receptor. The last two residues ($V^{4.61}$ and $P^{5.35}$) are mutated into more hydrophilic amino acids ($Y^{4.61}$ and $S^{5.35}$) in the human V_{1a} receptor (Fig. 1) and may provide a molecular explanation for the preferred binding of d[Cha[4]]AVP to the human V_{1b} subtype.

Again, this hypothesis was experimentally challenged by engineering human V_{1a} mutants ($Y186V^{4.61}$, $S213P^{5.35}$) bearing V_{1b} residues at the proposed 4.61 and 5.35 positions. As observed for the V_{1b} mutants, the V_{1a} mutants were correctly expressed on CHO cell membranes and exhibited nanomolar affinities for [^{3}H]AVP and maximal binding capacities ranging from 0.8–3.1 pmol [^{3}H]AVP specifically bound·mg^{-1} protein (Table 2 and Fig. 4). Yet, none of the single mutations significantly altered their binding affinity for d[Cha[4]]AVP (Table 3 and Fig. 5). However, the V_{1a} double mutant $Y186V^{4.61}$/$S213P^{5.35}$ resembles much more the V_{1b} receptor in its binding properties for d[Cha[4]]AVP with a much higher affinity of the peptide analog for the double mutant than for the wild-type V_{1a} receptor (Table 3). The $Y^{4.61}V$ mutation also weakly, but significantly, increased the affinity of the selective V_{1b} antagonist SSR149415 to the V_{1a} mutant. Strikingly, the $S^{5.35}P$ change affected SSR149415 binding only when presented together with the $Y^{4.61}V$ mutation. Last, the binding properties of the selective V_{1a} agonist F 180 or antagonist SR49059 were almost unchanged by any of the two mutations either alone or in combination (Table 3).

Mutating residues 4.61 and 5.35 affected more the functional properties of the human V_{1a} receptor as compared with binding parameters. Both single mutants were much more efficient than the wild-type V_{1a} receptor in stimulating phospholipase C by AVP or d[Cha[4]]AVP. Yet these effects were of weak amplitude (Table 4, Fig. 6). In contrast to our previous observation concerning d[Cha[4]]AVP binding properties, the double mutant did not confer any significant functional gain with respect to the single mutants.

DISCUSSION

A precise mapping of molecular interactions between peptide ligands and their receptors is a prerequisite for designing nonpeptide agonists for therapeutic applications. Taking advantage of the high-resolution structure of bovine rhodopsin (3), the only G protein-coupled receptor crystallized to date, we have developed homology models for two AVP receptor subtypes (V_{1a}, V_{1b}) in an explicit hydrated phospholipid environment and docked AVP and a recently described analog (d[Cha[4]]AVP) to each receptor model.

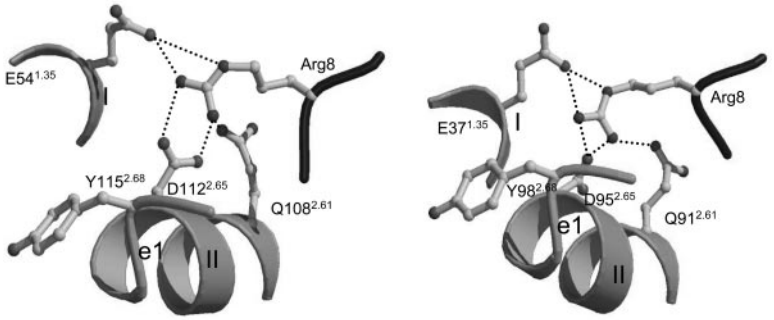

Fig. 3. Close-Up View of the Interaction of Arg8 Residue of AVP with Human V_{1a} (*Left Panel*) and V_{1b} Receptors (*Right Panel*)

The two TM helices (I and II) as well as the first extracellular loop (e1) at the vicinity of Arg8-contacting residues are displayed by *gray ribbons* and *tube*, respectively. The Arg8 main chain and side chain atoms of AVP are displayed by a *dark tube* and *ball-and-sticks*, respectively. V_{1a} amino acids are labeled according to the SwissProt numbering with the Ballesteros numbering indicated in *superscript*.

AVP is proposed to interact quite similarly with V_{1a} and V_{1b} receptor subtypes (Fig. 2, A and B) in agreement with previously described site-directed mutagenesis-guided mapping of the AVP binding site in the latter receptors (8, 9, 14). To experimentally challenge the yet undisclosed molecular partners of arginine 8 residue of AVP, the two negatively charged residues ($E^{1.35}$ and $D^{2.65}$) in close contact with arginine 8 (Fig. 3, A, B) were mutated to alanine in the human V_{1b} receptor. As predicted, binding of [^{3}H]AVP to the mutant receptors was significantly decreased both for the $E^{1.35}$A and to a lesser extend for the $D^{2.65}$A mutations (Table 2). Because both residues are fully conserved in all V_{1a} and V_{1b} receptor subtypes (Fig. 1), it is likely that the herein predicted interaction is a common feature of AVP recognition by the latter subtypes. The present model and its experimental validation also exclude the possibility that the neighboring $Y^{2.68}$ amino acid in V_{1a} and V_{1b} receptors directly interacts with Arg8, as previously reported in earlier recognition models (10), because the $Y^{2.68}$A mutation has no influence on AVP binding to the V_{1b} mutated receptor (Table 2). This negatively charged spot delineated by $E^{1.35}$ and $D^{2.65}$ is also used by other peptide agonists, especially $E^{1.35}$, which seems to be a common anchor to all ligands tested herein whatever their selectivity for individual subtypes (Tables 3 and 5). Lysine vasopressin for which the arginine 8 has been replaced by a lysine is also sensitive to both mutations, which can be easily explained by lysine's potential to develop ionic interactions with the two negatively charged residues. To further evidence the direct interaction between arginine 8 and $E^{1.35}$/$D^{2.65}$, we then tested an AVP analog (Phe^{3}OT: CYFQNCPLG-NH_2) for which arginine has been replaced by a leucine at position 8 (Table 5). As expected from the present 3-D model, the $E^{1.35}$A and $D^{2.65}$A mutations have much less consequences on the binding affinity of the latter analog to the mutant V_{1b} receptor. First, the binding affinity of Phe^{3}OT to the wild-type V_{1b} receptor is considerably decreased (K_i, ~100 nM) illustrating the significant contribution of arginine 8 to the overall binding affinity (recall K_d value of [^{3}H]AVP, Table 2). Second, both mutations have only a weak effect on Phe^{3}OT binding, confirming that residues 1.35 and 2.65 of the receptor and 8 of the ligand are in probable close proximity.

Quite surprisingly, both mutations also decrease the binding affinity of a nonpeptidic V_{1b} antagonist

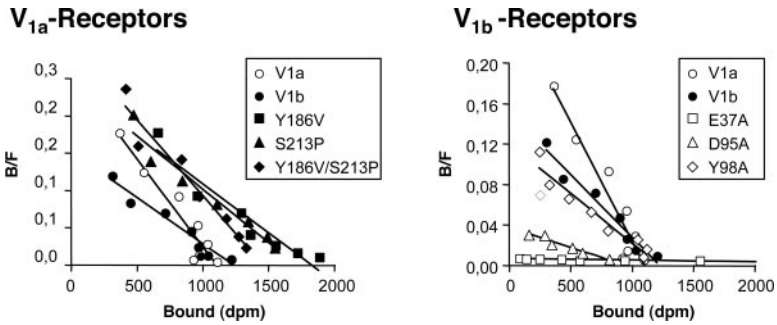

Fig. 4. Binding Properties of V_{1a} and V_{1b} Wild-Type and Corresponding Mutated Vasopressin Receptors for [^{3}H]AVP

Membrane from CHO cells transiently transfected with wild-type or mutated vasopressin receptors were incubated with increasing amounts of [^{3}H]AVP as described in *Materials and Methods*. Scatchard representation of saturation binding curves illustrated were representative of at least three distinct experiments each performed in triplicate. B/F, Bound/free; dpm, disintegrations per minute.

Table 2. Binding Properties of Wild-Type (wt) and Mutated Human Vasopressin Receptors for [^{3}H]AVP

Receptor	K_d (nM)	B_{max} (fmol/mg protein)
V_{1b} Receptors		
wt	0.43 ± 0.06	2244 ± 315
E37A$^{1.35}$	21.7 ± 2.5[a]	519 ± 91
D95A$^{2.65}$	1.6 ± 0.5[a]	507 ± 54
Y98A$^{2.68}$	0.57 ± 0.08	574 ± 25
V_{1a} Receptors		
wt	0.27 ± 0.06	1262 ± 327
Y186V$^{4.61}$	0.34 ± 0.08	2460 ± 82
S213P$^{5.35}$	0.43 ± 0.11	3174 ± 307
Y186V$^{4.61}$ / S213P$^{5.35}$	0.14 ± 0.02	802 ± 195

Binding assays were performed on membranes from CHO cells transiently transfected with human wild-type (wt) or mutated vasopressin receptors as described in *Materials and Methods*. The K_d and the B_{max} of each vasopressin receptor were calculated from Scatchard representation of dose saturation experiments illustrated in Fig. 4. Data are the mean ± SEM of at least three independent experiments each performed in triplicate.

[a] Significantly different from corresponding wild-type receptor value ($P < 0.05$).

Table 4. Coupling Properties of Wild-Type (wt) and Mutated Human Vasopressin Receptors to Phospholipase C

Receptor	K_{act} (nM) AVP	K_{act} (nM) d[Cha^4]AVP
V1b Receptors		
wt	0.88 ± 0.36	0.72 ± 0.07
E37A$^{1.35}$	373 ± 99[a]	n.d.
D95A$^{2.65}$	41 ± 10[a]	n.d.
V1a Receptors		
wt	0.67 ± 0.13	72.7 ± 15.2
Y186V$^{4.61}$	0.20 ± 0.03[a]	14.7 ± 2.3[a]
S213P$^{5.35}$	0.17 ± 0.09[a]	29.2 ± 9.4[a]
Y186V$^{4.61}$ / S213P$^{5.35}$	0.14 ± 0.01[a]	17.5 ± 2.1[a]

Phospholipase C assays were performed on CHO cells transiently transfected with human wild-type or mutated-vasopressin receptors. K_{act} values for AVP and d[Cha^4]AVP were obtained from dose-response curves illustrated in Fig. 6 as described in *Materials and Methods*. Results are the mean ± SEM of at least three distinct experiments each performed in triplicate. n.d., Not determined.

[a] Significantly different from corresponding wild-type receptor value ($P < 0.05$).

(SSR149415, Table 3) the previously mapped binding site of which (18) only partially overlap with the herein defined AVP binding region and is far away from the E$^{1.35}$-D$^{2.65}$ spot (Fig. 7). The effect of both above reported mutations on the binding of SSR149415 is difficult to rationalize from the present interaction model because direct molecular interactions between ligand and mutated residues are unlikely. During this work, the same E$^{1.35}$A mutation has been described for the V_{1a} receptor subtype and reported to dramatically decrease AVP binding and signaling but also to have no influence on the affinity of the selective V_{1a} nonpeptidic antagonist SR49059 (25). The binding site of SR49059 to the human V_{1a} receptor has already been mapped by our laboratory (19) and demonstrated to largely overlap that of the V_{1b} antagonist SSR149415 (18). At present, we have no clear explanation for the differential consequences of E$^{1.35}$A mutation on V_{1a} and V_{1b} nonpeptidic antagonists. Among possible explanations, this precise mutation may result in subtle conformational changes remotely affecting the antagonist binding site in the V_{1b} subtype.

To furthermore challenge the herein described 3-D models, we took advantage of the fine selectivity profile of a recently described V_{1b} peptide agonist (d[Cha^4]AVP), an analog of dAVP ([deamino-cys1]arginine vasopressin) (20) for which glutamine 4 has been changed to cyclohexylalanine (Cha) and which exhibits a 70-fold higher affinity for the V_{1a} subtype than for the V_{1b} subtype (Table 3). Our 3-D

Table 3. Binding Properties of Wild-Type (wt) and Mutated Human Vasopressin Receptors for Selective AVP Analogs

Receptor	Agonist			Antagonist	
	d[Cha^4]AVP	F180	dDAVP	SSR149415	SR49059
V1b Receptors					
wt	0.93 ± 0.34	662 ± 285	14.2 ± 1.35	0.73 ± 0.11	218 ± 91
E37A$^{1.35}$	187 ± 40[a]	n.d.	1926 ± 302[a]	>10,000[a]	n.d.
D95A$^{2.65}$	8.3 ± 0.8[a]	n.d.	7.7 ± 0.8[a]	9.6 ± 1.6[a]	n.d.
Y98A$^{2.68}$	2.8 ± 0.3[a]	n.d.	24.1 ± 2.62[a]	2.35 ± 0.02[a]	n.d.
V1a Receptors					
wt	65.3 ± 10.9	1.76 ± 0.34	n.d.	41 ± 3	0.89 ± 0.21
Y186V$^{4.61}$	43.4 ± 8.2	3.3 ± 0.4[a]	n.d.	19.2 ± 4.9[a]	0.64 ± 0.12
S213P$^{5.35}$	54.3 ± 12.3	4.5 ± 0.9[a]	n.d.	43.1 ± 6.4	1.36 ± 0.29
Y186V$^{4.61}$ / S213P$^{5.35}$	3.3 ± 0.4[a]	0.92 ± 0.07	n.d.	2.4 ± 0.6[a]	0.33 ± 0.12

Binding assays were performed on membrane from CHO cells transiently transfected with human wild-type or mutated-vasopressin receptors. K_i values for unlabeled vasopressin analogs were calculated from dose-displacement curves illustrated in Fig. 5. Data are the mean ± SEM of at least three different experiments each performed in triplicate. n.d., Not determined.

[a] Significantly different from corresponding wild-type vasopressin receptor value ($P < 0.05$).

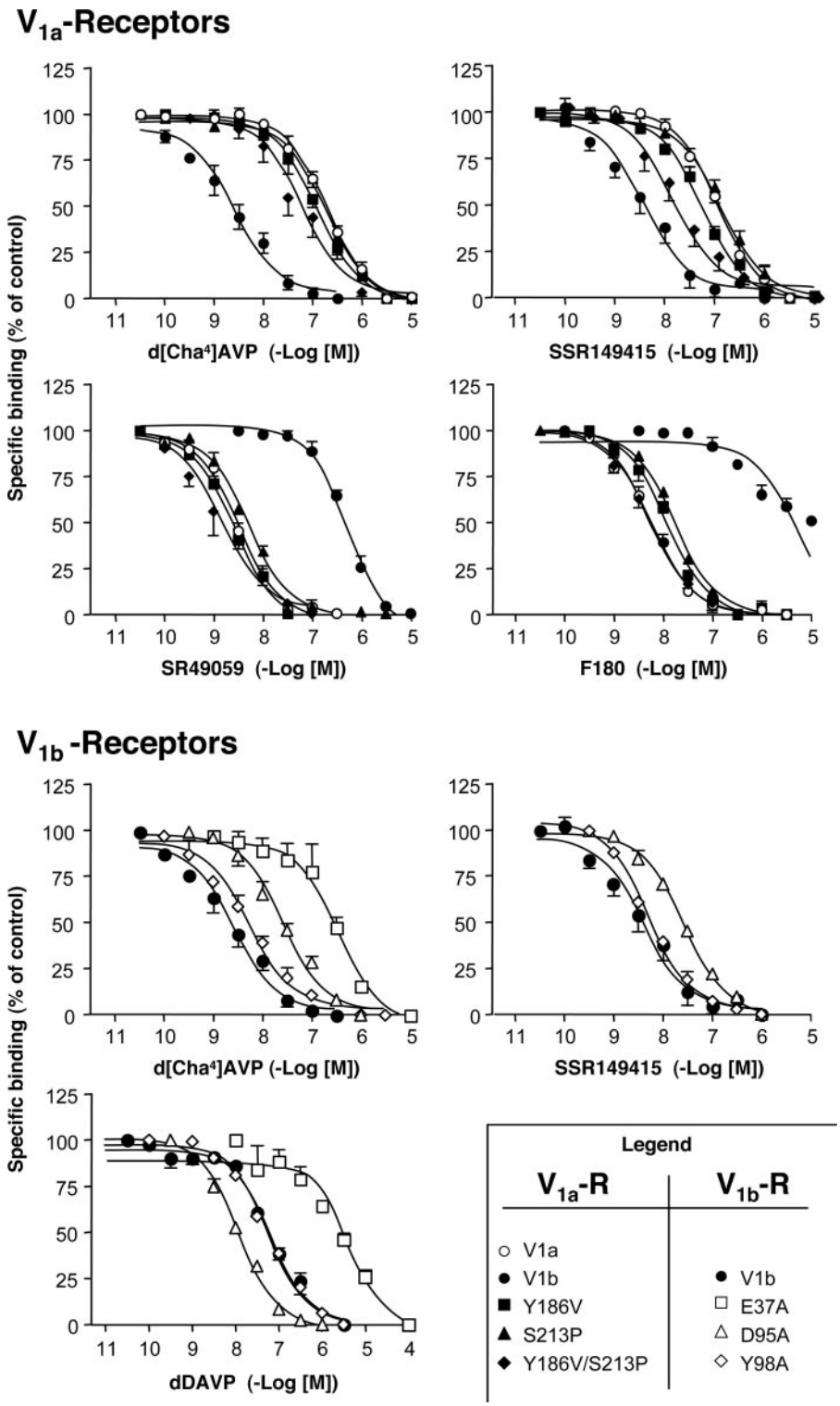

Fig. 5. Binding Properties of V_{1a} and V_{1b} Wild-Type and Corresponding Mutated Vasopressin Receptors for Selective Vasopressin Analogs

Membrane from CHO cells transiently transfected with wild-type or mutated vasopressin receptors were incubated with 1.5 nM to 15 nM [^{3}H]AVP according to the receptors considered: vehicle (control), increasing amounts of unlabeled vasopressin analogs (total binding), or with 1 μM unlabeled AVP (nonspecific binding). Specific binding were calculated in each experimental condition and expressed as percent of control specific binding. Results are the mean ± SEM of at least three distinct experiments, each performed in triplicate.

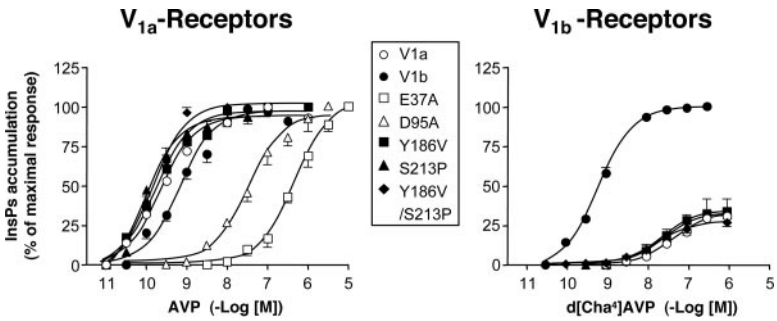

Fig. 6. Coupling Properties of V_{1a} and V_{1b} Wild-Type and Corresponding Mutated Vasopressin Receptors to Phospholipase C

CHO cells transiently transfected with wild-type or mutated vasopressin receptors were labeled with 1 μCi myo-[^{3}H]inositol as described in *Materials and Methods*. Cells were further incubated with either increasing amounts of AVP or d[Cha^4]AVP. Total IPs accumulated were extracted, counted, and expressed as percent of the maximal response induced by 1 μM AVP. Results are the mean ± SEM of at least three independent experiments each performed in triplicate.

models suggest that the fourth residue of the peptide ligand is accommodated by a pocket delineated both by four conserved residues among the AVP receptor family ($K^{3.29}$, $V^{3.33}$, $Q^{4.60}$, and $Y^{5.38}$; Fig. 8) and two variable amino acids ($V^{4.61}$ and $P^{5.35}$). A comparative observation of the sequence alignment (Fig. 1) and 3-D models (Fig. 8) clearly shows that the above-described pocket is significantly more polar in V_{1a} ($Y^{4.61}$, $S/T^{5.35}$) than in V_{1b} receptors ($V^{4.61}$, $P^{5.35}$). Therefore, it is logical that AVP analogs exhibiting hydrophobic residues are the most selective for the V_{1b} receptor subtype (20). To further validate this hypothesis, the two variable residues in the human V_{1a} receptor were mutated to their V_{1b} counterparts (Y186V, S213P). The two single and the double mutation had no effect on AVP binding (Table 3) because AVP does not discriminate between both subtypes, probably because of a tight hydrogen bond between Gln4 side chain and the conserved $Q^{4.60}$ (Table 1). The K_i of the selective V_{1b} agonist d[Cha^4]AVP was also not really modified by single mutations, but a drastic gain in affinity was observed for the double mutant (Table 3), thus confirming our starting hypothesis. It is likely that single mutations in this plastic hydrophobic subsite are compensated by slight conformational rearrangements that do not occur upon double mutation. Interestingly, the coupling properties of the mutant receptors to phospholipase C were already affected by single mutations (Table 4) and much closer to that of wild-type V_{1b} than wild-type V_{1a} receptor. Contrary to our previous observations, the double mutation does not here confer a better V_{1b} pharmacological profile to the V_{1a} double mutant (Table 4).

Table 5. Binding Properties of Wild-Type (wt) and Mutated Human V_{1b} Receptors, and of Human and Rat V_2 Vasopressin Receptors for Selected Agonists

Receptor	Ligand		
	LVP	Phe^{3}OT	d[Cha^4]AVP
Human V_{1b} (wt)	1.13 ± 0.06	101.5 ± 24.2	0.93 ± 0.34
Human V_{1b} (E37A$^{1.35}$)	17.0 ± 4.1	148.0 ± 42.5	187 ± 40
Human V_{1b} (D95A$^{2.65}$)	9.36 ± 0.63	169 ± 16	8.3 ± 0.8
Human V_2 (wt)	3.3 ± 0.3	n.d.	750 ± 120[a]
Rat V_2 (wt)	3.7 ± 0.5	n.d.	12.8 ± 2.8[a]

Binding assays were performed as described in legend of Table 3. n.d., Not determined.
[a] From Ref. 26.

The present sequence alignment (Fig. 1) also provides a good explanation for the d[Cha^4]AVP pharmacological species differences previously observed for vasopressin V_2 receptors (26). Hence, the only difference in the above-reported Cha4 binding pocket between human and rat V_2 subtypes lies precisely at position 5.35 (Fig. 1). In the human V_2 subtype, position 5.35 is a bulky and positively charged amino acid (Arg), which is probably not suited to accommodate a bulky hydrophobic side chain at position 4 of the peptide ligand. Mutation to a smaller and more hydrophobic residue (Leu) in the rat V_2 receptor is therefore beneficial to the binding of d[Cha^4]AVP (Table 5). Conversely, AVP analogs with smaller polar side chains (*e.g.* lysine vasopressin) do not distinguish human from rat V_2 receptors (Table 5). It is difficult from the present data to explain the selective binding of d[Cha^4]AVP to the human V_{1B} receptor *vs.* human OT receptor (26). Strikingly, AVP itself does not distinguish between those receptors. These subtle differences are probably beyond the accuracy of the current homology models. It is still possible that the human OT receptor has slightly different orientation and kinks of the seven helices when bound to d[Cha^4]AVP.

The proposed interaction models, however, should be valuable to design novel selective agonists, notably by focusing on some positions (5.42 and 7.39 for example) which vary across the AVP receptor family and which also explain the selective binding of nonpeptide V_{1b} antagonists (18).

In conclusion, receptor modeling of human AVP receptors in complex with AVP and d[Cha^4]AVP, a se-

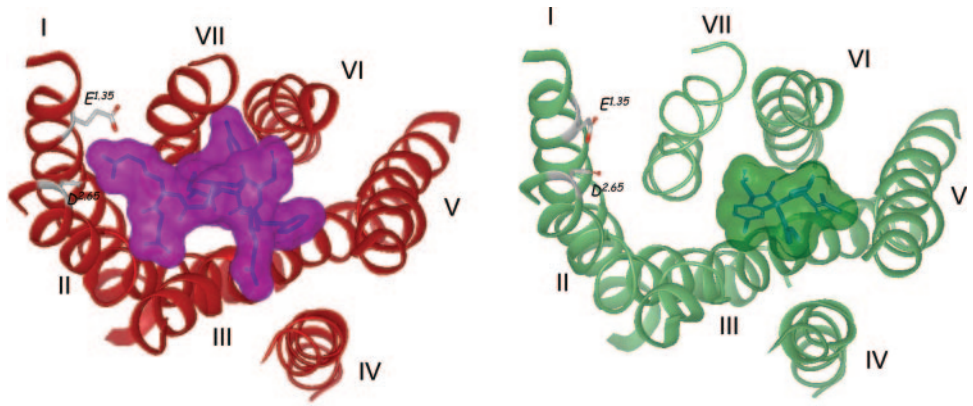

Fig. 7. Proposed 3-D Model of Interaction of AVP (*Left Panel*, This Work) and SSR149415 (*Right Panel*, Ref.18) to the Human V_{1b} Receptor

Only TM helices (labeled from I–VII) are shown as *red ribbons* for sake of clarity. Two negatively-charged residues ($E^{1.35}$ and $D^{2.65}$) the mutation of which decreases the binding affinity of the two ligands (Tables 2 and 3) are shown by *white* (carbon) and *red* (oxygen) *sticks*. The ligand (*blue sticks*) is shown along with its molecular surface (*magenta* for AVP, *green* for SSR14915). The figure was prepared and rendered with VIDA2 (OpenEye Scientific Software, Santa Fe, NM).

lective V_{1b} agonist, shed light on putative molecular interactions between the peptide hormone and its receptors. Validation of the computational models by studying the binding and coupling properties of a few mutants on V_{1a} and V_{1b} receptor unambiguously demonstrate that arginine-8, a very important residue for ligand binding, interacts with a set of negatively charged amino acids ($E^{1.35}$, $D^{2.65}$) at V_{1a} and V_{1b} receptor subtypes. Moreover, a rational explanation to the V_{1b}-selective binding of d[Cha^4]AVP is proposed and confirmed by site-directed mutagenesis. Altogether, the refined 3-D models of V_{1a} and V_{1b} human receptors in complex with peptide agonists should facilitate the identification of selective and nonpeptidic V_{1a} and V_{1b} agonists as pharmacological but also therapeutic tools.

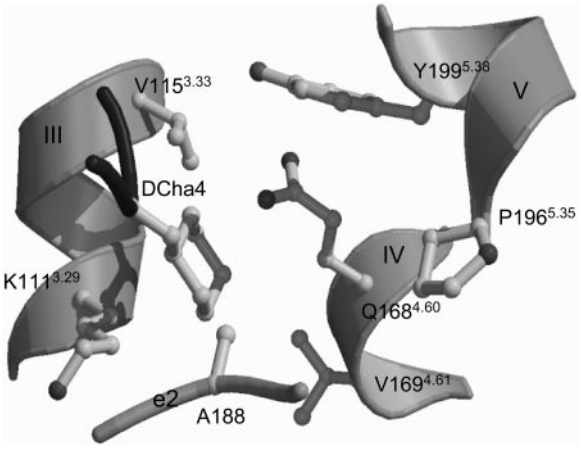

Fig. 8. Close-Up View of the Interaction of Cha4 Residue of d[Cha^4]AVP with the Human V_{1b} Receptor

The three TM helices (III, IV, V) as well as the second extracellular loop (e2) at the vicinity of Cha4-contacting residues are displayed by *gray ribbons* and *tube*, respectively. The Cha4 main chain and side chain atoms of AVP are displayed by a *dark tube* and *ball-and-sticks*, respectively. V_{1b} amino acids are labeled according to the SwissProt numbering with the Ballesteros numbering indicated in *superscript*.

MATERIALS AND METHODS

Residue Numbering and Nomenclature

The residue numbering proposed by Ballesteros *et al.* (27) was used throughout this manuscript. It allows an unambiguous comparison of TM residues for any class A GPCR by assigning position 50 to a fully conserved amino acid at each TM (Asn for TMI, Asp for TMII, Arg for TMIII, Trp for TMIV, Pro for TMs V–VII; see Fig. 1) and numbering other amino acids according to this reference residue. Residue x.y is thus the amino acid describing position y of TMx. For purposes of clarification, amino acids from the peptide ligands will be labeled using a three-letter code whereas receptor residues will be labeled using a single-letter code.

Alignment of Amino Acid Sequences

The amino acid sequences of human and rat AVP and OT receptor subtypes were retrieved from the Swiss-Prot database (accession nos: human V_{1a} receptor, P37288; rat V_{1a} receptor, P30560, human V_{1b} receptor, P47901; rat V_{1b} receptor, P48974; human V_2 receptor, P30518; rat V_2 receptor, Q00788; human OT receptor, P30559; rat OT receptor, P70536) and aligned to the sequence of bovine rhodopsin (accession no. P02699) using the in-house developed GPCRmod program (21) focusing on transmembrane (TM) domains only. The alignment of the amino and carboxy-terminal domains as well as of the intra- and extracellular loops was realized using ClustalW (28). A slow pairwise alignment using BLOSUM matrix series (29) and a gap opening penalty of 15.0 were chosen for aligning the amino acid sequences to the sequence of bovine rhodopsin.

Modeling the AVP-Bound Conformation of Human V_{1a} and V_{1b} Receptors

3-D ground-state models of human V_{1a} and V_{1b} receptors have recently been reported by our group (17–19). To achieve an agonist-bound model from an antagonist-bound model, we followed, for each receptor subtype, a five-step protocol as proposed by Bissantz *et al.* (17). In a first step, only the first and third extracellular loops between helices 2 and 3, and helices 6 and 7, respectively, were included in a preliminary model. In a second step, AVP was docked to this preliminary model using the Gold 2.1 program (30). For each of the 10 independent genetic algorithm (GA) runs, a maximum number of 1000 GA operations was performed on a single population of 50 individuals. Operator weights for crossover, mutation, and migration were set to 100, 100, and 0, respectively. To allow poor nonbonded contacts at the start of each GA run, the maximum distance between hydrogen donors and fitting points was set to 5 Å, and nonbonded van der Waals energies were cut off at a value equal to kij (well depth of the van der Waals energy for the atom pair i,j). To further speed up the calculation, the GA docking was stopped when the top three solutions were within 1.5 Å rmsd. If this criterion is met, we can assume that these top solutions represent a reproducible pose for the ligand. It should be observed that the starting conformation of AVP was modeled from the x-ray structure of neurophysin-bound OT (23). In a third step, the receptor-AVP complex was minimized with AMBER8.0 (31) using the AMBER03 force field to relax the structure and to remove steric bumps. In a fourth step, the extracellular loop 2 between helices 4 and 5 and the N-terminal region were added to the model through a simple knowledge-based loop search procedure as previously described (17). The disulfide bridge present between $Cys^{3.25}$ and a conserved Cys in the extracellular 2 loop was kept unchanged with respect to the x-ray structure of bovine rhodopsin (3). After the heavy atoms were modeled, all hydrogen atoms were added, and the protein coordinates were then minimized again with AMBER. The minimizations were carried out by 1000 steps of steepest descent followed by conjugate gradient minimization until the rms gradient of the potential energy was lower than 0.05 kcal/mol·Å. A twin cutoff (10.0, 15.0 Å) was used to calculate nonbonded electrostatic interactions at every minimization step, and the nonbonded pair list was updated every 25 steps. A distance-dependent ($\varepsilon = 4r$) dielectric function was used. Last, the complex was embedded in a preequilibrated lipid bilayer consisting in 70 molecules of palmitoyloleoylphosphatidylcholine and solvated by 11,588 TIP3P water molecules (box dimensions: 86.6 * 93.1 * 78.0 Å) as recently described by Urizar *et al.* (32). A short minimization was applied to the complex embedded in the hydrated lipid bilayer using AMBER8.0 and applying a positional harmonic constraint of 50 kcal/mol·Å on Cα carbons. A 1-nsec constant pressure molecular dynamics (MD) simulation was then applied to the entire system. Periodic boundaries and Particle Mesh Ewald summation were considered to treat electrostatic interactions. All bonds involving hydrogen atoms were frozen with the SHAKE algorithm, thus enabling the selection of a 2-fsec integration step. During the first 250 psec, the α-carbons were constrained as previously described, and the temperature was linearly increased from 0 to 300 K. In the productive part of the MD simulation (last 750 psec), the temperature was fixed to 300 K by coupling to a heat bath using a coupling constant of 0.2. All atoms were free to move, energies and coordinates were saved every 10 psec. The analysis of the MD trajectories was realized using the ptraj module of AMBER8.0.

Automated Docking of d[Cha^4]AVP

The docking of d[Cha^4]AVP to the two receptor models was done as described for AVP.

Site-Directed Mutagenesis

All the mutations were generated into the human V_{1a} or V_{1b} receptor sequence. The human V_{1a} and V_{1b} cDNA inserted into the pRK5 expression vector was kindly provided by Dr. B. Mouillac. Amino acid replacements were generated by PCR using the QuikChange Site-Directed Mutagenesis kit (Stratagene, La Jolla, CA), as previously described (26). For single amino acid replacements of mutants E37A, D95A, and Y98A, cDNA of the wild-type human V_{1b} receptor was used as the template with the appropriate mutated oligonucleotide primers. For replacements of Y186V and S213P mutants, cDNA from V_{1a} receptor was used as the template. The double mutant Y186V/S213P was generated as described above using cDNA of the Y186V mutant as the template and mutated oligonucleotide primers corresponding to the S213P mutation. Each construct was transformed, amplified in the *Escherichia coli* DH5-α strain (Invitrogen, Cergy-Pontoise, France), and then purified with the QIAprep Spin Miniprep Kit (QIAGEN, Courtaboeuf, France). All the mutations were verified by sequencing (Genome Express, Meylan, France).

cDNA Expression of Wild-Type and Mutant Vasopressin Receptors and Cell Culture

The human V_{1a} and V_{1b} wild-type receptors were stably expressed in CHO cells as previously described (26). The mutants of the human V_{1a} or V_{1b} receptors were transiently expressed in CHO cells by electroporation. Briefly, the cells (10^7/0.3 ml) were resuspended in an electroporation buffer (50 mM K_2HPO_4; 20 mM $C_2H_3KO_2$; 20 mM KOH; pH 7.4) with 20 μg of carrier DNA (pRK5 expression vector without insert) and 0.5–2.0 μg of the expression vector containing the mutated receptor cDNA and 40 mM $MgSO_4$. They were then incubated for 20 min at room temperature before being pulsed [280 V, 950 microfarads; Bio-Rad Apparatus (Bio-Rad Laboratories, Hercules, CA)]. CHO cells expressing the wild-type and mutated vasopressin receptors were plated in 150-mm Petri dishes or 24-well plates depending upon the experiment to be conducted. Cells were cultured 48 h at 37 C in DMEM supplemented with 10% fetal calf serum, 2 mM L-glutamine, 500 U/ml penicillin and streptomycin, and nonessential amino acids (1×) in an atmosphere of 95% air and 5% CO_2. Sodium butyrate (3 mM) was added in the incubation medium for the last 24 h.

Membrane Preparation

CHO cells, stably or transiently transfected with wild-type or mutated receptors, were washed twice in PBS without $CaCl_2$ and $MgCl_2$, harvested in lysis buffer (15 mM Tris-HCl, pH 7.4; 2 mM $MgCl_2$; 0.3 mM EDTA), polytron homogenized, and centrifuged at 44,000 × *g* for 20 min at 4 C. Pellets were washed in a Buffer A (50 mM Tris-HCl, pH 7.4; 3 mM $MgCl_2$) and centrifuged at 44,000 × *g* for 20 min at 4 C. Membranes were resuspended in a small volume of Buffer A. Protein concentration was determined by the method of Bradford with the Bio-Rad protein assay kit and using BSA as a standard. Membranes were stored at −80 C before use.

Binding Experiments

Membrane binding assays were performed as previously described using [^{3}H]AVP as radioligand. Membranes (5–10 μg protein) were incubated 60 min. at 30 C in a medium containing: 50 mM Tris-HCl, pH 7.4; 3 mM $MgCl_2$; 1 mg·ml^{-1} BSA; and 0.01 mg·ml^{-1} leupeptin. Affinity (K_d) of [^{3}H]AVP for the wild-type and the mutated vasopressin receptors was determined by saturation experiments using concentrations of labeled vasopressin ranging from 0.1 to 30 nM. For each concentration of radioligand, total and nonspecific binding

was determined in absence or presence, respectively, of 1 μM unlabeled AVP. The affinities (K_i) of the unlabeled analogs were determined by competition experiments. Briefly, depending upon the receptors studied, 0.5 to 15 nM of [^{3}H]AVP was added in the incubation medium with or without increasing amounts of the unlabeled analogs to be tested (total binding). Nonspecific binding was determined under the same experimental conditions in the presence of 1 μM unlabeled AVP. The radioactivity found associated with plasma membranes was determined by filtration through glass microfiber filters (GF/C Series; Whatman International Ltd., Maidstone, UK). Specific binding was calculated and expressed as percent of the maximal binding capacity determined without unlabeled analog. K_i values were calculated from the dose-displacement curves fitted with the Cheng and Prusoff equation.

IP Assays

Total IP accumulation was determined as previously described. Briefly, CHO cells stably or transiently transfected with the wild-type and the mutated receptors were grown for 24 h in DMEM supplemented with 10% fetal calf serum. Cells were further incubated for another 24-h period in a serum and inositol-free medium supplemented with 1μCi·ml^{-1} myo-[^{3}H]-inositol and 3 mM sodium butyrate. Cells were then washed twice with a Hanks' buffered saline (HBS) medium, equilibrated at 37 C in HBS for 30 min, and incubated for 15 min in HBS supplemented with 15 mM LiCl, 1 mg·ml^{-1} glucose, 1 mg·ml^{-1} BSA and 2.1 g·liter^{-1} $NaHCO_3$. Cells were further stimulated for 15 min with increasing concentrations of the analogs to be tested. Reaction was stopped by adding perchloric acid (5% vol/vol, final concentration). IPs accumulated were extracted and purified on Dowex AG1-X8 anion exchange chromatography column as previously described (26) and counted.

Chemicals

All reagents used were of analytical grade. Most standard chemicals were purchased from Sigma (St. Louis, MO), Roche Molecular Biochemicals (Mannheim, Germany), or Merck & Co., Inc. (Darmstadt, Germany), unless otherwise indicated. AVP came from Bachem (Bubendorf, Switzerland). [^{3}H]AVP (60–80 Ci/mmol) was from PerkinElmer Life Sciences (Courtaboeuf, France). SSR149415 and SR49059 were from Sanofi-Aventis Laboratories (Toulouse, France). DMEM, penicillin-streptomycin, L-glutamine, and nonessential amino acids were purchased from Invitrogen (Cergy Pontoise, France). Inositol-free DMEM came from ICN Biochemicals (Orsay, France). Dowex AG1-X8 format form 200–400 mesh was purchased from Bio-Rad Laboratories, Inc. (München, Germany). d[Cha^4]AVP was synthesized by Dr. M. Manning (College of Medicine, University of Toledo, OH).

Data Analysis

The radioligand binding data were analyzed by GraphPad Prism (GraphPad Software, Inc., San Diego, CA). The dissociation constants (K_d) of the radioligands were determined according to the Scatchard linearization of the saturation curve obtained (33). The inhibitory dissociation constants (K_i) for unlabeled analogs were calculated from binding competition experiments according to the Cheng and Prusoff equation (34): $K_i = IC_{50} \times (1+[L]/K_d)$, where IC_{50} is the concentration of unlabeled analog leading to half-maximal inhibition of specific binding, [L] the concentration of the radioligand present in the assay, and K_d its affinity for the receptor studied. Concentrations of analog leading to half-maximal stimulation (K_{act}) or inhibition (K_{inact}) of IPs accumulation were calculated from functional studies using GraphPad Prism. Results are expressed as the mean ± SEM of the number of distinct experiments indicated.

Acknowledgments

We thank Sanofi-Aventis for providing us selective nonpeptidic vasopressin antagonists. The Computational Centers at Montpellier (CINES, Centre Informatique National de l'Enseignement Supérieur) and Orsay (IDRIS, Institut du Développement des Ressources Informatiques Scientifiques) are gratefully acknowledged for allocation of computing time. D.R. thanks Dr. Michael T. Bowers for providing us the structure of Zn^{2+}-bound OT. We also thank M. Passama for drawing the illustration and Dr. M. Manning for his generous gift of d[Cha^4]AVP.

Received May 11, 2006. Accepted October 24, 2006.

Address all correspondence and request for reprints to: Dr. Didier Rognan, Centre Nationale de la Recherche Scientifique Université Louis Pasteur Unité Mixte de Recherche 7175-LC1, 74 Route du Rhin, F-67401 Illkirch, France. E-mail: didier.rognan@pharma.u-strasbg.fr.

This work was supported by the European Commission for the Marie-Curie fellowship to J.R (HPMF-CT-2002-02141), the Basque Country University (Bilbao, Spain; Grant 9/UPV-00042.310-15852/2004), and "Secretaría de Estado de Educación y Universidades" (Madrid, Spain) for the fellowship to M.T.; A.P. received a fellowship from Sanofi-Aventis.

Current address for J.R.: Centre d'Etudes et de Recherche sur le Médicament de Normandie, Unité Propre de Recherche et de l'Enseignement Supérieur, Equipe d'Accueil 3915, Département de Modélisation Moléculaire, Université de Caen Basse-Normandie, Normandie, France.

REFERENCES

1. Barberis C, Mouillac B, Durroux T 1998 Structural bases of vasopressin/oxytocin receptor function. J Endocrinol 156:223–229
2. Barberis C, Durrroux T, Mouillac B, Guillon G, Seyer R, Hibert M, Tribollet E, Manning M 1999 Molecular pharmacology of AVP and OT receptors and therapeutic potential? Drugs New Perspect 12:279–298
3. Palczewski K, Kumasaka T, Hori T, Behnke CA, Motoshima H, Fox BA, Trong IL, Teller DC, Okada T, Stenkamp RE, Yamamoto M, Miyano M 2000 Crystal structure of rhodopsin: a G protein-coupled receptor. Science 289:739–745
4. Tyndall JD, Pfeiffer B, Abbenante G, Fairlie DP 2005 Over one hundred peptide-activated G protein-coupled receptors recognize ligands with turn structure. Chem Rev 105:793–826
5. Hibert M, Hoflack J, Trumpp-Kallmeyer S, Mouillac B, Chini B, Mahe E, Cotte N, Jard S, Manning M, Barberis C 1999 Functional architecture of vasopressin/oxytocin receptors. J Recept Signal Transduct Res 19:589–596
6. Hausmann H, Richters A, Kreienkamp HJ, Meyerhof W, Mattes H, Lederis K, Zwiers H, Richter D 1996 Mutational analysis and molecular modeling of the nonapeptide hormone binding domains of the [Arg8]vasotocin receptor. Proc Natl Acad Sci USA 93:6907–6912
7. Cotte N, Balestre MN, Phalipou S, Hibert M, Manning M, Barberis C, Mouillac B 1998 Identification of residues responsible for the selective binding of peptide antagonists and agonists in the V2 vasopressin receptor. J Biol Chem 273:29462–29468
8. Mouillac B, Chini B, Balestre MN, Elands J, Trumpp-Kallmeyer S, Hoflack J, Hibert M, Jard S, Barberis C 1995

The binding site of neuropeptide vasopressin V1a receptor. Evidence for a major localization within transmembrane regions. J Biol Chem 270:25771–25777
9. Thibonnier M, Coles P, Conarty DM, Plesnicher CL, Shoham M 2000 A molecular model of agonist and nonpeptide antagonist binding to the human V(1) vascular vasopressin receptor. J Pharmacol Exp Ther 294:195–203
10. Chini B, Mouillac B, Ala Y, Balestre MN, Trumpp-Kallmeyer S, Hoflack J, Elands J, Hibert M, Manning M, Jard S, Barberis C 1995 Tyr115 is the key residue for determining agonist selectivity in the V1a vasopressin receptor. EMBO J 14:2176–2182
11. Phalipou S, Cotte N, Carnazzi E, Seyer R, Mahe E, Jard S, Barberis C, Mouillac B 1997 Mapping peptide-binding domains of the human V1a vasopressin receptor with a photoactivatable linear peptide antagonist. J Biol Chem 272:26536–26544
12. Phalipou S, Seyer R, Cotte N, Breton C, Barberis C, Hibert M, Mouillac B 1999 Docking of linear peptide antagonists into the human V(1a) vasopressin receptor. Identification of binding domains by photoaffinity labeling. J Biol Chem 274:23316–23327
13. Thibonnier M, Coles P, Thibonnier A, Shoham M 2002 Molecular pharmacology and modeling of vasopressin receptors. Prog Brain Res 139:179–196
14. Cotte N, Balestre MN, Aumelas A, Mahe E, Phalipou S, Morin D, Hibert M, Manning M, Durroux T, Barberis C, Mouillac B 2000 Conserved aromatic residues in the transmembrane region VI of the V1a vasopressin receptor differentiate agonist vs. antagonist ligand binding. Eur J Biochem 267:4253–4263
15. Slusarz MJ, Gieldon A, Slusarz R, Ciarkowski J 2005 Analysis of interactions responsible for vasopressin binding to human neurohypophyseal hormone receptors-molecular dynamics study of the activated receptor-vasopressin-Gα systems. J Pept Sci 12:180–189
16. Slusarz MJ, Sikorska E, Slusarz R, Ciarkowski J 2006 Molecular docking-based study of vasopressin analogues modified at positions 2 and 3 with N-methylphenylalanine: influence on receptor-bound conformations and interactions with vasopressin and oxytocin receptors. J Med Chem 49:2463–2469
17. Bissantz C, Bernard P, Hibert M, Rognan D 2003 Protein-based virtual screening of chemical databases. II. Are homology models of G-protein coupled receptors suitable targets? Proteins 50:5–25
18. Derick S, Pena A, Durroux T, Wagnon J, Serradeil-Le Gal C, Hibert M, Rognan D, Guillon G 2004 Key amino acids located within the transmembrane domains 5 and 7 account for the pharmacological specificity of the human V1b vasopressin receptor. Mol Endocrinol 18:2777–2789
19. Tahtaoui C, Balestre MN, Klotz P, Rognan D, Barberis C, Mouillac B, Hibert M 2003 Identification of the binding sites of the SR49059 nonpeptide antagonist into the V1a vasopressin receptor using sulfydryl-reactive ligands and cysteine mutants as chemical sensors. J Biol Chem 278: 40010–40019
20. Cheng LL, Stoev S, Manning M, Derick S, Pena A, Mimoun MB, Guillon G 2004 Design of potent and selective agonists for the human vasopressin V1b receptor based on modifications of [deamino-cys1]arginine vasopressin at position 4. J Med Chem 47:2375–2388
21. Bissantz C, Logean A, Rognan D 2004 High-throughput modeling of human G-protein coupled receptors: amino acid sequence alignment, three-dimensional model building, and receptor library screening. J Chem Inf Comput Sci 44:1162–1176
22. Attwood TK 2001 A compendium of specific motifs for diagnosing GPCR subtypes. Trends Pharmacol Sci 22: 162–165
23. Rose JP, Wu CK, Hsiao CD, Breslow E, Wang BC 1996 Crystal structure of the neurophysin-oxytocin complex. Nat Struct Biol 3:163–169
24. Liu D, Seuthe AB, Ehrler OT, Zhang X, Wyttenbach T, Hsu JF, Bowers MT 2005 Oxytocin-receptor binding: why divalent metals are essential. J Am Chem Soc 127: 2024–2025
25. Hawtin SR, Wesley VJ, Simms J, Argent CC, Latif K, Wheatley M 2005 The N-terminal juxtamembrane segment of the V1a vasopressin receptor provides two independent epitopes required for high affinity agonist binding and signaling. Mol Endocrinol 19:2871–2881
26. Derick S, Cheng LL, Voirol MJ, Stoev S, Giacomini M, Wo NC, Szeto HH, Ben Mimoun M, Andres M, Gaillard RC, Guillon G, Manning M 2002 [1-deamino-4-cyclohexylalanine] arginine vasopressin: a potent and specific agonist for vasopressin V1b receptors. Endocrinology 143: 4655–4664
27. Ballesteros JA, Weinstein H 1995 Integrated methods for the construction of three-dimensional models and computational probing of structure-function relations of G protein-coupled receptors. Methods Neurosci 25: 366–428
28. Thompson JD, Higgins DG, Gibson TJ 1994 CLUSTAL W: improving the sensitivity of progressive multiple sequence alignment through sequence weighting, position-specific gap penalties and weight matrix choice. Nucleic Acids Res 22:4673–4680
29. Henikoff S, Henikoff JG 1992 Amino acid substitution matrices from protein blocks. Proc Natl Acad Sci USA 89:10915–10919
30. Verdonk ML, Cole JC, Hartshorn MJ, Murray CW, Taylor RD 2003 Improved protein-ligand docking using GOLD. Proteins 52:609–623
31. Case DA, Darden TA, Cheatham I TE, Simmerling CL, Wang J, Duke RE, Luo R, Merz KM, Wang B, Pearlman DA, Crowley M, Brozell S, Tsui V, Gohlke H, Mongan J, Hornak V, Cui G, Beroza P, Schafmeister C, Caldwell JW, Ross WS, Kollman PA 2004 AMBER 8. San Francisco: University of California
32. Urizar E, Claeysen S, Deupi X, Govaerts C, Costagliola S, Vassart G, Pardo L 2005 An activation switch in the rhodopsin family of G protein-coupled receptors: the thyrotropin receptor. J Biol Chem 280:17135–17141
33. Weder HG, Schildknecht J, Lutz RA, Kesselring P 1974 Determination of binding parameters from Scatchard plots. Theoretical and practical considerations. Eur J Biochem 42:475–481
34. Cheng Y, Prusoff WH 1973 Relationship between the inhibition constant (Ki) and the concentration of inhibitor which causes 50 per cent inhibition (I50) of an enzymatic reaction. Biochem Pharmacol 22:3099–3108
35. Kraulis P 1991 MOLSCRIPT: a program to produce both detailed and schematic plots of protein structures. J Applied Crystallogr 24:946–950
36. Merritt EA, Murphy MEP 1994 Raster3D Version 2.0. A program for photorealistic molecular graphics Acta Crystallogr D 50:869–873
37. Surgand JS, Rodrigo J, Kellenberger E, Rognan D 2006 A chemogenomic analysis of the transmembrane binding cavity of human G-protein-coupled receptors. Proteins 62:509–538

***Molecular Endocrinology* is published monthly by The Endocrine Society (http://www.endo-society.org), the foremost professional society serving the endocrine community.**